THE UNIVERSITY *of* EDINBURGH

Edinburgh Research Explorer

Defining the microglia response during the time course of chronic neurodegeneration

Citation for published version:
Vincenti, JE, Murphy, L, Renault, K, McColl, BW, Cancellotti, E, Freeman, TC & Manson, JC 2016, 'Defining the microglia response during the time course of chronic neurodegeneration', *Journal of Virology*, vol. 90, no. 6, pp. 3003-3017. https://doi.org/10.1128/JVI.02613-15

Digital Object Identifier (DOI):
10.1128/JVI.02613-15

Link:
Link to publication record in Edinburgh Research Explorer

Document Version:
Peer reviewed version

Published In:
Journal of Virology

Publisher Rights Statement:
Copyright © 2015 Vincenti et al.
This is an open-access article distributed under the terms of the Creative Commons Attribution 4.0 International license.

General rights
Copyright for the publications made accessible via the Edinburgh Research Explorer is retained by the author(s) and / or other copyright owners and it is a condition of accessing these publications that users recognise and abide by the legal requirements associated with these rights.

Take down policy
The University of Edinburgh has made every reasonable effort to ensure that Edinburgh Research Explorer content complies with UK legislation. If you believe that the public display of this file breaches copyright please contact openaccess@ed.ac.uk providing details, and we will remove access to the work immediately and investigate your claim.

Download date: 24. Aug. 2022

JVI Accepted Manuscript Posted Online 30 December 2015
J. Virol. doi:10.1128/JVI.02613-15
Copyright © 2015 Vincenti et al.
This is an open-access article distributed under the terms of the Creative Commons Attribution 4.0 International license.

Accepted Manuscript Posted Online
Journal of Virology
JVI
Journal of Virology

Defining the microglia response during the time course of chronic neurodegeneration

Running title: Microglia in neurodegeneration

James E. Vincenti, Lita Murphy, Kathleen Grabert, Barry W. McColl, Enrico Cancellotti, Tom C. Freeman[±] and Jean C. Manson[±*]

The Roslin Institute and Royal (Dick) School of Veterinary Studies, University of Edinburgh, Easter Bush, Midlothian EH25 9RG, United Kingdom

[±] Joint senior authors

Corresponding author:

*Professor Jean Manson: jean.manson@roslin.ed.ac.uk

Conflict of Interests
None of the authors have any conflict of interest relating to this study

Authors Contributions

JV, EC, TF and JM designed the study, JV conducted the research, JV, TF and JM analysed the data, JV, TF and JM wrote the manuscript. BM, KR, LM provided tools and expertise and provided a valuable review of the manuscript.

36 pages, 9 figures, 1 supplementary table
Abstract 248 words, Text 5470

Accepted Manuscript Posted Online

Journal of Virology

JVI

1 **Abstract**

2 Inflammation has been proposed as a major component of neurodegenerative diseases
3 although the precise role it plays has yet to be defined. We have examined the role of key
4 contributors to this inflammatory process, microglia, the major resident immune cell
5 population of the brain, in a prion disease model of chronic neurodegeneration. Initially, we
6 performed an extensive reanalysis of a large study of prion disease, where the
7 transcriptome of mouse brains had been monitored throughout the time-course of disease.
8 Our analysis has provided a detailed classification of the disease-associated genes based on
9 cell type of origin and gene function. This revealed that the genes up-regulated during
10 disease, regardless of the strain of mouse or prion protein, are expressed predominately by
11 activated microglia. In order to study the microglia contribution more specifically we
12 established a mouse model of prion disease in which the 79A murine prion strain was
13 introduced by an intraperitoneal route into BALB/cJ$^{Fms\text{-}EGFP/-}$ mice, which express Enhanced
14 Green Fluorescent Protein (EGFP) under control of the *c-fms* operon. Samples were taken at
15 time points during disease progression and histological analysis of the brain and
16 transcriptional analysis of isolated microglia was carried out. The analysis of isolated
17 microglia revealed a disease specific, highly pro-inflammatory signature in addition to an up-
18 regulation of genes associated with metabolism and respiratory stress. This study strongly
19 supports the growing recognition of the importance of microglia within the prion disease
20 process and identifies the nature of the response through gene expression analysis of
21 isolated microglia.

22

23

Journal of Virology

Accepted Manuscript Posted Online
JVI Journal of Virology

24 **Importance**

25

26 Inflammation has been proposed as a major component of neurodegenerative diseases. We
27 have examined the role of key contributors to this inflammatory process, microglia, the
28 major resident immune cell population of the brain, in a murine prion disease model of
29 chronic neurodegeneration. Our study demonstrates that genes up-regulated throughout
30 the disease process, are expressed predominately by microglia. A disease specific highly
31 pro-inflammatory signature was observed in addition to an up-regulation of genes
32 associated with metabolism and respiratory stress. This study strongly supports the growing
33 recognition of the important contribution of microglia to a chronic neurodegenerative
34 disease process.

35

36 **Key Words**

37 Microglia, Neurodegeneration, Prion

38

39

40 **Introduction**

41 Over several decades the neuron has been subject to the majority of research into protein
42 misfolding diseases, but it is now apparent that glial cells are important players in the
43 neurodegenerative process. Many protein misfolding diseases including Alzheimer's disease,
44 Parkinson's disease and prion diseases demonstrate activation of glial cells in the brain
45 during the course of disease alongside accumulation of misfolded protein but the precise
46 role of the glial cells in the disease process is not known (1-4). Transmission of prion agents

Journal of Virology

Accepted Manuscript Posted Online

Journal of Virology

JVI

47 to mice provides an excellent model for studying the timing of events during a chronic
48 process of a neurodegeneration associated with a misfolded protein. The time of inoculation
49 defines the starting point for the disease process and highly reproducible characteristics of
50 mouse-adapted prions include accumulation of a misfolded host protein, gliosis, neuronal
51 loss, distribution of brain lesions and the end point of terminal disease. Activation of glial
52 cells, both astrocytes and microglia, has been extensively documented as an early event in
53 the pathogenesis of protein misfolding diseases, occurring well before the onset of clinical
54 disease (1, 5-7).
55
56 Microglia are the major resident immune cell in the brain and in steady-state are considered
57 a heterogeneous population with density differences across brain regions (8). They display
58 region dependant functional signatures, which are enhanced further by age (9). Under
59 normal conditions microglia adopt a 'resting' phenotype where they continually survey their
60 immediate environment with extended processes (10).
61
62 Following detection of a pathological insult or any disturbance to homeostasis, microglia
63 adapt their phenotype from 'resting' to 'activated' whereby they modify both morphology
64 and biological function (10-12). Activated microglia have diverse functional phenotypes
65 dependent on the nature of the stimuli that are not readily apparent from their
66 morphology, and include a much wider repertoire than the classically defined M1 and M2
67 phenotypes (13-16). It has also been proposed that microglia can readily switch from one
68 phenotype to another (17-19) and are sensitive to peripheral immune system
69 communication (20-22). It is also clear that a complicated interconnected network of CNS

Journal of Virology

Accepted Manuscript Posted Online

Journal of Virology

JVI

70 cells contribute to the activated 'profile' adopted by microglia with signalling from both
71 astrocytes and neurons having particular impact (23-26).
72
73 The change of microglia from a resting to an activated state is one of the first pathological
74 features of prion disease long before there is any evidence of neurodegeneration. Activated
75 microglia are widely distributed in the brain and are thought to express low levels of
76 inflammatory cytokines but high levels of transforming growth factor beta 1 (TGFB1) and
77 prostaglandin E2 (PGE2) (7, 27).
78
79 This study aims to investigate the role of microglia through detailed analysis of their
80 morphology and gene expression during the course of prion disease thereby providing new
81 insights into the pathophysiology of neurodegenerative disease. We have used a prion
82 disease agent as a model of neurodegeneration and taken an unbiased whole genome
83 expression analysis approach, which has allowed us to provide an insight into the molecular
84 processes central to microglia during the neurodegeneration, and highlight how this may
85 impact disease development. A strong myeloid association was attributed to disease
86 associated genes identified in our reanalysis supporting the growing recognition of the
87 importance of microglia within the disease process. To further clarify microglial contribution
88 we isolated microglia from prion infected mice and analysed their gene expression profile.
89

Journal of Virology

Accepted Manuscript Posted Online

Journal of Virology

JVI

90 **Material and methods**

91 ***Reanalysis of Hwang et al. (2009) Data***

92 The Hwang dataset (28) was downloaded from http://prion.systemsbiology.net. Quality
93 control of these data was performed by Fios Genomics Ltd. (Edinburgh, Scotland) using the
94 ArrayQualityMetrics (29) and 32 microarrays were removed due to poor quality leaving 386,
95 both infected and uninfected, for reanalysis. The removal of arrays did not affect the overall
96 balance of the dataset with a mean average of 2.5 ± 0.08 SE arrays per time point. Data
97 normalisation was performed using the Robust Multiarray Average (RMA) expression
98 measure (30).
99
100 Initial inspection of the data showed that there were no age-related trends present in the
101 control animal data and these were not included in further analyses. Data from prion
102 infected animals were loaded into BioLayout *Express*^{3D} (31) and a Pearson correlation matrix
103 calculated, comparing the expression data from each probeset on the array against all other
104 probesets ($P^2/2$ pairwise calculations, where P is the number of probesets).
105
106 A threshold of $r \geq 0.75$ was used and the resultant correlation graph visualised. To identify
107 groups of co-expressed genes, the graph was clustered using the graph-based Markov
108 clustering (MCL) algorithm (32) with the inflation value set at 2.2. The expression profile of
109 each cluster was inspected, and clusters of genes differentially expressed during disease
110 were isolated and individual gene profiles examined. Those with an unconvincing profile, i.e.
111 their expression was weak or unrelated to disease progression, were removed. This left a

Journal of Virology

Accepted Manuscript Posted Online

Journal of Virology

JVI

Journal of Virology

112 dataset comprising 492 genes in which there was high degree of confidence that their
113 expression was up-regulated during disease.
114
115 ***Determination of Cell Type of Origin and Function of Disease-associated Transcripts***
116 Cell origin was determined with reference to existing datasets. A dataset was compiled
117 from data derived from a number of published studies and included microglia, macrophage
118 and osteoclast myeloid populations (33, 34); purified neuronal populations derived from the
119 cortex (cholecystokinin^{+ve}, cholinergic, layer 5a, layer 5b, layer 6, prepronociceptin^{+ve}); the
120 striatum (dopamine receptor subtype-1 medium spiny, dopamine receptor subtype-2
121 medium spiny) and the cerebellum (basket, Golgi, purkinje, stellate, unipolar brush) and
122 astrocytes, Bergman glia and oligodendrocyte populations (35, 36). Finally, datasets
123 derived from macrophage cultures cultured with lipopolysaccharide (LPS) bacterial
124 endotoxin (37) were included to allow for the identification of those genes associated with
125 activation of the innate immune system. Following normalisation of the data, the 492 genes
126 demonstrating differential expression in response to prion disease were identified in the
127 composite dataset through matching of gene symbols, and incorporated into an expression
128 file. Within BioLayout *Express*^{3D} each gene could then be assessed for their expression in
129 one or more of these cell types.
130
131 Gene ontology enrichment was determined by uploading the Affymetrix chip ID of the
132 disease-associated genes to the online Ensembl Biomart data mining tool
133 (ensembl.org/biomart) using the *Mus musculus* genes dataset (Ensembl Genes 66). Filters
134 were applied restricting results to the Affymetrix 430 2.0 chip probe sets. To increase

Accepted Manuscript Posted Online

Journal of Virology

JVI

135 accuracy for correct selection of function, filters for gene ontology evidence code, domain
136 and name were applied, with experimental evidence codes preferred.
137
138 ***Animals and Treatment***
139 Groups of male and female BALB/cJ$^{Fms\text{-}EGFP/-}$ mice, expressing enhanced green fluorescent
140 protein (EGFP) under control of the *c-fms* operon (part of the *Csfr1* promoter) (38), were sex
141 matched and housed under standard conditions in groups of three to five. Food and water
142 access was *ad libitum*. All mouse experiments were reviewed and approved by the local
143 ethical review committee and performed under license from the UK Home Office in
144 accordance with the United Kingdom Animal (Scientific Procedures) Act 1988. Mice aged at
145 16 weeks old were challenged by an intraperitoneal (i.p.) route with 0.02 ml of 1% w/v (in
146 physiological saline) 79A infected or normal brain material (NBr) for control. At time points
147 35, 100, 150 and 200 days post-inoculation (dpi) mice were sacrificed (9 per group for
148 immunohistochemical analysis and 4 per group for microglial extraction). All remaining
149 mice (12 and 8 per group respectively), were assessed for clinical signs of prion disease from
150 150 dpi, and incubation times were calculated according to previously described protocols
151 (39). These mice were sacrificed during terminal disease, or earlier if welfare required.
152 Tissue sections from these mice were assessed for spongiform degeneration following
153 previously described procedures by a scientist blinded to experimental design (40).
154
155 ***Tissue Preparation and Immunohistochemical Analysis***
156 Brains were removed at the selected time points. Those to be used for
157 immunohistochemistry were perfusion fixed with saline followed by 4% paraformaldehyde

Journal of Virology

Accepted Manuscript Posted Online

Journal of Virology

JVI

158 (PFA), pH 7.4. Brain tissue was embedded in paraffin and cut into sections (6 µm). Antigen
159 retrieval was performed in an autoclave at 121°C for 15 min in dH_2O and then incubated in
160 formic acid (98%) for 10 min at room temperature. Endogenous peroxidase was blocked
161 with 1% H_2O_2 (Sigma-Aldrich) in methanol for 10 min. All sections were blocked with
162 serum-free protein block (Dako) or normal goat serum prior to incubation with the primary
163 antibody. Sections were immunostained with monoclonal antibody (MAb) 6H4 (Prionics)
164 recognizing residues 143-151 of murine PrP (0.5 µg ml^{-1}) (41). Negative control slides were
165 treated overnight with mouse immunoglobulin control (Invitrogen). Antibody binding was
166 detected with Vector ABC kit (Vector laboratories) and visualized with 3,3,-
167 diaminobenzidine chromogen. All sections were counterstained with haematoxylin.

168 Brains for microglia morphology assessment were removed and immersed in 4% PFA for 24
169 h, rinsed in Hank's balanced salt solution (HBSS) before incubating for a further 24 h in 20%
170 sucrose solution at 4^oC. Tissues were rinsed with HBSS and snap frozen in isopentane at -
171 40^oC. Brains for microglial extraction were immersed in cold HBSS prior to processing (see
172 microglial isolation procedure).

173

174 ***Quantification of Microglia Morphology/ Phenotype***

175 Frozen brain tissue was sectioned at 25 µm on a freezing block microtome and sequential
176 sections 300 µm apart were taken for analysis. Quantification of microglia activation status
177 was established on cellular aggregation and morphology observed in BALBcJ$^{Fms\text{-}EGFP/-}$ sections
178 based on the average number of microglia per 0.05 mm^2. Images for cell quantification were
179 captured as a 50 optical slice z-stack at x10 magnification (Zeiss Plan-Neofluar 10x/0.30

Journal of Virology

Accepted Manuscript Posted Online

Journal of Virology

JVI

180 objective) and compiled into a composite image using ImageJ software 1.48a.
181 Quantification of EGFP cell number was performed using particle analysis within ImageJ.
182 Microglia radius was performed on x10 Z stack compiled (reporting Z stacks) images taken at
183 x40 magnification (Zeiss Plan-Neofluar x40 / 1.30 objective) captured from three standard
184 locations within four brain regions: the dentate gyrus, cerebellum, medulla and thalamus.
185 There was a minimum of 3 mice per group and additional images were recorded on adjacent
186 sections if the total number of EGFP expressing microglia was below 50. Euclidean distance
187 mapping was utilised to quantify changes in morphology and was performed using the
188 'region of interest' function within ImageJ.
189

190 ***Microglial isolation procedure***

191 Brains harvested for microglial extraction were placed in cold HBSS and diced before
192 processing immediately. Brains were dissociated using a GentleMACS™ Dissociator (Miltenyi
193 Biotec) and Neural Tissue Dissociation Kit P (Miltenyi Biotec). The final cell pellet was re-
194 suspended in 16 ml 35% Isotonic Percoll, split between two 15 ml tubes and carefully
195 overlaid with 5 ml ice cold 0.1% DEPC treated HBSS. The resulting Percoll gradient was
196 centrifuged at 400 g for 45 min at 4°C. The pellets were then suspended and recombined
197 into a final volume of 5 ml ice cold 0.1 % DEPC treated HBSS. Cells were pelleted at 400 g
198 for 5 min at 4°C using no brake, re-suspended in 90 µl ice cold MACs buffer (Miltenyi
199 Biotec), 10 µl CD11b (microglia) microbeads (Miltenyi Biotec) and incubated at 4°C for 15
200 min with gentle rotation. Following incubation with microbeads, the cell suspension was
201 washed in 1 ml ice cold MACs buffer at 300 g for 5 min at 4°C then re-suspended in 500 µl

Journal of Virology

Accepted Manuscript Posted Online

Journal of Virology

JVI

202 ice cold MACs buffer. Cells were passed through magnetised LS columns (Miltenyi Biotec)
203 following the manufacturer's protocol.
204

205 ***Verification of Microglial Purity***

206 A subset of isolated cells predicted to be microglia were stained with PE anti-mouse CD11b
207 (Cambridge Bioscience) and APC anti-mouse CD45 (Cambridge Bioscience). Isotype controls
208 were prepared using PE Rat IgG2b (Cambridge Bioscience) and APC Rat IgG2a (Cambridge
209 Bioscience) and a subset of unstained cells served both as negative control and verification
210 of correct BALB/cJ$^{\mathit{Fms\text{-}EGFP/-}}$ genotype. Cell viability was determined using SYTOX® Blue dead
211 cell stain (Thermofischer Scientific). All cell samples were analysed on a BD FACS Aria IIIu 4-
212 laser/11 detector cell sorter running BD FACSDiva™ software (BD Biosciences). Subsequent
213 analysis of FACS data was also performed using Summit v4.3 software (Dako/Beckham
214 Coulter).
215

216 ***Microarray Analysis of Isolated Microglia***

217 Isolated microglia cells were treated with TRIzol® Reagent (Life Technologies) according to
218 manufacturer's protocol. Total RNA quality was checked on an Agilent 2100 Bioanalyzer.
219 RNA samples with RIN value of >7.0 were passed as suitable for analysis and two
220 representative samples at each time-point for control and disease were taken forward for
221 analysis. RNA processing was handled by Ark Genomics (The Roslin Institute & R(D)SVS).
222 RNA was converted to amplified double-stranded cDNA containing biotin using the NuGen
223 Ovation picoSL WTA labelling kit (NuGen). The cDNA samples were hybridised to Affymetrix

Journal of Virology

Accepted Manuscript Posted Online
Journal of Virology
JVI

224 Mouse Gene 1.1 arrays on a GeneTitan instrument (Affymetrix). Data was quality controlled,
225 RNA normalised and subjected to network analysis as described above.
226
227 **Results**

228 ***The neurodegenerative disease process is associated with an inflammatory response***
229 ***which is microglial in origin***

230 Initially, we performed a reanalysis of the data produced by Hwang *et al.* (2009): a
231 transcriptomics analysis of brains of multiple strains of mice infected with different prion
232 strains sampled at various stages of disease progression. These analyses were performed
233 with a view to identifying genes associated with neurodegenerative disease progression.
234 The Hwang data from diseased animals were analysed within BioLayout *Express*^{3D}. A
235 correlation graph was generated using a Pearson threshold of $r \geq 0.75$, consisting of 21,550
236 nodes with 1,253,332 edges (Figure 1A). Clustering with MCL yielded 416 clusters. Each
237 cluster represented genes that share a high degree of co-expression. The expression profile
238 of the majority of the clusters revealed they had an expression profile that was not linked to
239 the disease process. Two major clusters of genes did however exhibit an expression profile
240 that increased with disease progression in all animal/prion strain combinations (Figure 1B).
241 The largest of these clusters comprised 377 genes and a second contained 115 genes that
242 were notable for their increased activation in C57/Bl6 models (Figure 1B). Following manual
243 inspection of all individual profiles, a total of 492 genes associated with prion disease
244 development were identified (Supplementary Table 1). All genes in each cluster followed a
245 similar expression profile with an increase in expression starting at approximately half way
246 through the incubation period.

Journal of Virology

Accepted Manuscript Posted Online

Journal of Virology

JVI

247

248 Once disease association was determined, we next attempted to identify the cellular origin
249 for each of the 492 differentially expressed genes in question. This was done by examining
250 the expression of the disease-associated genes in the context of a panel of isolated cell
251 populations. Datasets were sourced from the GNFv3 cell atlas (33, 34), RNA TRAP (35, 36)
252 and serial macrophage cultures subjected to LPS (37). This revealed that 315 out of the 492
253 differentially expressed genes were solely or at least predominately expressed by myeloid
254 populations, thereby indicating the majority were likely expressed by microglia within the
255 brain. In contrast, 147 of the genes were expressed by multiple cell types, whilst only 30
256 were found to be specific to astrocytes, oligodendrocytes and neurons collectively (Figure 2).
257 The original study by Hwang et al., (2009) identified 333 differentially expressed genes. By
258 overlaying these 333 genes onto our chosen external datasets within BioLayout *Express*^{3D} it
259 was found that 158 of the 333 genes were attributed to a myeloid origin. A further 18 were
260 attributed to non-myeloid cell types. The remaining genes were classed as generic, implying
261 the origin could be any cell within the brain and as such do not rule out a microglial
262 component.

263

264 ***Histological Analysis of Microglial Activation and PrP Deposition***

265 Following the identification of the predominantly myeloid origin of the prion disease
266 signature, we chose next to confirm this observation by performing an analysis of microglia
267 isolated from diseased brains. Our aim was to verify these findings and to obtain a more
268 detailed analysis of the activation of microglia during disease. To do this we chose a mouse

Journal of Virology

Accepted Manuscript Posted Online

269 passaged prion agent 79A, inoculated into BALB/cJ $^{Fms-EGFP/-}$ mice by an intraperitoneal route
270 with 0.02 ml of 1% w/v 79A brain homogenate as our model.
271
272 Clinical disease onset occurred 198.5 +/- 1.0 (SEM) dpi with signs including lethargy, hair
273 unkempt/loss and hunching all reported. Terminal disease occurred 229 +/- 3.6 dpi.
274 Pathological analysis of the vacuolation in the brain of terminal animals (n=6) confirmed
275 clinical disease and indicated that vacuolation was widespread by terminal stage of disease
276 presenting as typical for the 79A prion strain (42, 43).
277
278 PrP deposition assessed by immunohistochemistry using the 6H4 antibody was first
279 detected in the infected mice at 150 dpi and restricted to the medulla (Figure 3A/B). PrP
280 assessment at the terminal stage of disease identified heavy accumulation of fine punctate
281 particles throughout the majority of the brain, strongest in the thalamus and extending into
282 the medulla. To a lesser extent, deposition was also observed within the hippocampus, but
283 it was only occasionally found within the cortex. This is the deposition pattern typically
284 associated with 79A disease progression (42, 44). Microglial activation was observed in the
285 same areas as PrP deposition at 150 dpi (Figure 3C/D). Microglia in the NBr inoculated
286 controls demonstrated ramified appearance and greater microglia separation at ~50 µm
287 (Figure 3E/F).
288
289 Microglia were identified during the course of disease using EGFP expression and a
290 quantitative analysis performed on their density and radius, as a measurement of
291 morphological changes typically associated with the activation of microglia. Comparison to
292 animals that had been inoculated with uninfected NBr homogenate, we observed at 150 dpi

Accepted Manuscript Posted Online
JVI Journal of Virology
Journal of Virology

293 an approximate 50% (p = 0.029) increase of microglial cell number per 0.05 mm^2, within the
294 medulla of 79A infected mice (Figure 4A). Similarly, at 200 dpi an increase of microglia of
295 approximately 50% (p = 0.02) was observed within the thalamus. The intercellular distance
296 of microglial in control and unaffected regions was approximately 70-100 µm, while within
297 affected regions this was reduced to approximately 25 µm (Figure 4B). Cellular microglial
298 activation was also defined by a marked increase in the diameter of the central body while
299 there is a reduction in the length and number of processes projecting from it (45). An
300 average length of approximately 30 µm was observed for thalamic microglia at 100 days,
301 while at 200 dpi this is reduced to an average of 20 µm, indicating morphology associated
302 with activation. The reduction in radius is matched with an increase in Euclidean distance
303 by 1 µm, similar to that seen in the microglia in the thalamus, and indicative of shorter
304 thicker processes and a larger central body (Figure 4C-E). Thus the pathological analysis
305 confirmed that microglial activation and PrP disease associated protein deposition occurs by
306 150 dpi in restricted regions of the brain, and during the course of disease both extend into
307 multiple brain regions. There was no evidence of either PrP deposition or microglial
308 activation at 100 days in this model.
309
310 ***Microglial activation profile***
311 Microglia were isolated at day 35, 100, 150 and 200 dpi from 79A inoculated and control
312 animals. Isolated cells were stained with CD11b and CD45 fluorochrome conjugated
313 antibodies and sorted by FACS to confirm purity (Figure 5A-D). Adult microglia are typically
314 shown as $CD11b^{High}$ and $CD45^{Low}$ (46) and the lower than expected CD11b forward and side
315 scatter may be attributed to competition for available antigen between the CD11b

Accepted Manuscript Posted Online

316 microbeads and CD11b-PE marker. The number of CD45^{high} cells, indicative of impurities in
317 the cell isolation process by monocyte contamination, was negligible. Non-specific binding
318 or auto-fluorescence was not observed. Cell viability was confirmed as 97% ± 0.43 SE.
319 Microglia purity was further confirmed from the expression profile of twenty cell-specific
320 genes representing the main cell groups found within the brain (Figure 5E). The presence of
321 CD11b^{positive} circulating or inflammatory monocytes was confirmed to be absent as
322 evidenced by the negligible expression of *Ly6c* or *Ccr2* (Supplementary Figure 1).
323
324 The process of isolation did not appear to adversely affect the microglia disease signature.
325 There was a clear difference between expression profiles of microglia isolated from diseased
326 mice and those collected from uninfected controls. Of note was the lack of increased
327 expression of metabolism genes that may be expected if cells were unduly stressed during
328 the isolation process. Staining with SYTOX® Blue also confirmed cells from both infected and
329 control animals were viable prior to RNA isolation. Additionally, on a bright field microscope,
330 isolated microglia presented with a rounded refractive appearance, indicative of healthy
331 viable cells.
332
333 RNA was extracted and microarray analysis was performed. Following this, the patterns of
334 gene expression were analysed within BioLayout *Express*^{3D}. The expression profile of each
335 cluster was individually checked to ensure familiarity with the dataset, and those with a
336 disease associated signature selected. This resulted in 741 genes that demonstrated an
337 increase in expression predominately at 200 dpi. The 741 genes were also organised into 2
338 large clusters which shared a very similar gene expression profile with a clear increase in
339 expression profile (shown averaged in Figure 6A). Animals inoculated with NBr material

Journal of Virology JVI Journal of Virology

Accepted Manuscript Posted Online

Journal of Virology

JVI

340 showed no significant change in expression throughout the corresponding period. Using the
341 741 genes of interest, a sample-to-sample (array) level graph within BioLayout *Express*^{3D} was
342 generated and confirmed the arrays from the 200 dpi time point had less correlation with
343 the rest of the samples (Figure 6B).
344
345 ***Gene Enrichment Analysis***

346 Enrichment analysis of the disease-associated microglial genes using the FuncAssociate 2.0
347 database (47), confirmed the enrichment ($p<0.001$) of the following functional gene
348 descriptions; translation, energy production, immune response, interferon response and cell
349 stress (Figure 7A). Immunological response comprised the single largest category in respect
350 to total gene number. The signature included transcripts associated with proteolysis, NFkB-
351 mediated cytokine cascades and innate immunity. The GO enrichment functional groups of
352 mitochondria, ribosome, cell stress, apoptotic process and proliferation confirmed the
353 presence of a significant metabolic signature associated with these genes.
354
355 Gene ontology was performed for each gene using the data made available on the Ensembl
356 Biomart database to allow for functional associations to be determined (Figure 7B). Just
357 under two thirds of the 741 identified differentially expressed genes were attributed to
358 metabolism and the maintenance of homeostasis. The correct determination of
359 differentially expressed metabolic genes to a specific cell type is only possible through the
360 type of isolated cell type analysis presented here. Metabolic genes are typically expressed
361 by all tissue cells types, making identification of the cellular origin from a mixed cell
362 population impossible. Genes that were related to the immune response comprised just

Journal of Virology

Accepted Manuscript Posted Online

Journal of Virology

JVI

363 under a quarter of the total. The 6% of genes associated with cytoskeletal changes and
364 migration were classed into their own groups respectively and included genes associated
365 with membrane reshuffling. This was to be expected as microglia are known to be highly
366 motile in the healthy brain environment (10). The increased expression of cytokines *Il1*, *Tnfa*
367 and *Csf1*, but not *Il6* or *Il10*, would suggest the response by microglia is lacking in the full
368 spectrum of cytokines expected from a classical form of activation via the myeloid
369 differentiation primary response 88 (MYD88)-dependant pathway (48). Pathway analysis of
370 this dataset within the Reactome database (49), revealed many of the elements of the
371 MYD88-independent pathway were represented by the differentially expressed genes
372 within this study. This is supported by the lack of differential expression of *Myd88* (Figure
373 7C). In addition, *Tgfb1* was not found to be differentially expressed by microglia during the
374 disease process (Figure 7D). Transcripts associated with Tgfb1 signalling, including Smad
375 anchor for receptor activation (*Zfyve9*), suppressor-of-cytokine-signalling 3, 4 and 5 (*Socs3-*
376 *5*) and ubiquitin specific peptidase 15 (*Usp15*) were also absent.
377
378 Determination of the sub-cellular component for each gene considered to be associated
379 with metabolism/homeostasis was performed from data obtained from the Ensembl
380 Biomart database. This enabled the location of many genes to be plotted onto a cellular
381 map and further organised by function (Figure 8). The identified cellular components
382 included a significant increase in expression of genes associated with ribosomes within the
383 rough endoplasmic reticulum and cytoplasm. Indeed, the bulk of the metabolic genes were
384 associated with the ribosomes, thereby implying an increase in ribosome numbers and/or
385 ribosome turnover, or an increase in protein synthesis. Also present was a significant

Journal of Virology

Accepted Manuscript Posted Online

Journal of Virology

JVI

386 concentration of genes associated with proteolysis, including proteasome based
387 ubiquitination.
388
389 Consistent with the increase in metabolic load were a considerable number of genes
390 associated with oxidative phosphorylation and energy production in mitochondria, including
391 subunits for cytochrome-c oxidase, NADH dehydrogenase and lactate dehydrogenases; the
392 latter associated with breakdown of increased levels of lactate in situations of respiratory
393 stress (50). Also observed were DNA repair processes including expression of poly(ADP-
394 ribosyl)ation-14 (*Parp14*); a potent transcriptional regulator and DNA damage-dependant
395 nuclear protein (51, 52).
396
397 The association of the identified genes of interest with a specific function outside
398 metabolism/homeostasis was plotted onto a cellular map using ontology data obtained
399 from the Ensembl Biomart database. This enabled the location of each gene to be
400 determined and further organised by function (Figure 9). The overall expression profile from
401 this set of genes is one of robust pro-inflammatory myeloid cell activation. The increased
402 expression of lysosomal-associated membrane protein, ATPase proton pumps and
403 numerous lysosomal enzymes including cathepsins, histocompatibility subunits and genes
404 involved in membrane restructuring, strongly support antigen presentation and are a
405 hallmark of classically activated innate immune cells. Increased expression of surface marker
406 transcripts *Cd48*, *Cd86*, *Ccl8*, *Cxcl9*, *Cxcl13*, and *Tlr2* was also observed and all are typically
407 associated with a pro-inflammatory classical activation phenotype (16, 53-55).
408

Journal of Virology

Accepted Manuscript Posted Online

Journal of Virology

JVI

409 **Discussion**

410 The dataset generated by Hwang, et al. (28) is uniquely placed among transcriptome
411 datasets as it is the first to be fully comprehensive in terms of prion-related disease models,
412 encompassing as it does multiple prion strains and host backgrounds. Our reanalysis of
413 these data using a correlation network-based approach in combination with a cell origin
414 classification system has given a unique, unbiased and informative whole genome approach.
415 This allows identification not only of a core set of genes involved, but also of cell types
416 associated with the neurodegenerative disease process. We identified a further 299 disease-
417 associated genes not reported in the original study by Hwang, et al. (28) (Table 1). The
418 original analysis focused on defining pathways associated with disease progression, which
419 speculated a prominent neuronal contribution to the disease signature. However our
420 reanalysis identified a large proportion of those previously identified genes to be of a
421 myeloid origin with a strong myeloid association being attributed to 315 out of the 492
422 disease associated genes. This supports the growing recognition of the importance of
423 microglia within the disease process. To further clarify microglial contribution we isolated
424 microglia from prion infected mice and analysed their gene expression profile.

425

426 Experimental differences between the current study and that of Hwang, et al. (28) including
427 route of infection, single cell type analysis and RNA amplification, potentially limit the ability
428 to directly compare the results of the two studies. Having said this 107 genes were seen to
429 be upregulated during disease progression in both studies and were primarily associated
430 with an innate immune response (Supplementary Figure 1). We adopted an intraperitoneal
431 route of infection as a "more natural" route of infection rather than the more commonly

Journal of Virology

Accepted Manuscript Posted Online

Journal of Virology

JVI

432 used intracranial route to ensure that microglial activation was the result of a response to
433 initial infection entering the CNS environment. With an intracranial route of infection the
434 microglial response may be complicated by the injection procedure resulting in what has
435 been termed as 'pre-priming' of microglia (56-58). A peripheral route would also
436 encapsulate any microglial response to systemic inflammation; observed in prion disease
437 following a peripheral route of infection (59), but not following an intracerebral route (60).
438 However both studies arrive at the same conclusion; prion disease is associated with a
439 chronic inflammatory response with microglia being central to the disease process.
440
441 The increase in levels of *Il1b*, *Tnfa* and *Csf1* strongly portray the microglial activation profile
442 as pro-inflammatory and not one of atypical down-regulation or resolution of inflammation
443 (61). The presence of a significant increase in transcripts involved with proteasome activity
444 and major-histocompatibility mediated antigen presentation, combined with expression of
445 *Cxcr3* ligand genes, offers a microglia activation state more akin to classically activated
446 macrophages. That said, the lack of expression of *Infγ*, *Il6* and *Il33* by microglia, all well-
447 defined pro-inflammatory cytokines (62-64) suggests an atypical inflammatory response.
448 Also of note, and crucial to the maintenance of a chronic response to inflammatory
449 cytokines, was that expression of *Nfkb1* remained stable despite an increase in expression
450 of NFKB1 inhibitors (*Nfκbia*, *Nfκbib* and *Nfκbie*) which have been shown to inhibit formation
451 of NFKB1 at the transcription stages (65).
452
453 The inflammatory phenotype typically associated with prion disease has been shown to be
454 remarkably anti-inflammatory and dominated by the anti-inflammatory growth factor Tgf-
455 β1 following injection by an intracerebral (66) or hippocampal stereotactic route (7, 61).

Journal of Virology

Accepted Manuscript Posted Online

Journal of Virology

JVI

456 Found in the healthy brain, Tgf-β1 is a constitutively expressed protein intricately involved in
457 microglia homeostasis (67-70). The lack of differential expression of *Tgfb1* within this
458 dataset, suggests a lack of active TGF-β1 mediated signalling as a significant contributor to
459 the disease response by microglia. There was also lack of significant increase in expression
460 of *Usp15*, *Zfyve9* or *Socs3-5,* indicating no increased translocation of SMAD2/3 proteins or
461 MAPK signalling; core intracellular complexes of the TGF-β1 signalling pathway (67, 71-73).
462 TGF-β1 is required for the correct function of the blood brain barrier, and is itself unable to
463 pass (74, 75). This therefore suggests that the increased expression of Tgf-β1 noted in other
464 studies, is either attributable to the intracerebral inoculation or expressed by another group
465 of cells from within the CNS.
466
467
468 Microglia are known to intricately interact with neurons (76-78), and numerous genes
469 associated with axon elongation, synapse regulation and neurotransmitter release were
470 observed to increase in expression within the isolated microglia dataset. This partners the
471 expression of many axon and synapse genes with microglia and adds them to the growing
472 body of evidence for microglial involvement in neuron regulation (79-83). It has been
473 proposed that microglia kill prion infected neurons in a manner dependent upon the
474 presence and degree of fibrillarity of misfolded protein (84). This single cell dataset supports
475 the generation of a neurotoxic response from microglia with increased expression of *Il1b,*
476 *Tnfa* and caspase-4 (*Casp4*) indicating active processing within caspase-1 mediated
477 inflammasomes (85-87). Other pro-inflammatory genes found within this dataset, and
478 reported to be neurotoxic, include matrix metalloproteinase 12 (*Mmp12*) (88) and
479 prostaglandin-endoperoxide synthase 2 (*Ptgs2*) (89). The latter is known to be expressed in

Journal of Virology

Accepted Manuscript Posted Online

JVI

Journal of Virology

480 prion disease (90, 91) and is a target of non-steroidal anti-inflammatory drugs (NSAIDs) used
481 in clinical trials to treat neurodegenerative diseases by inhibiting prostaglandin synthesis
482 (92).
483
484 Within this analysis microglia were shown to express a disease signature markedly more
485 pro-inflammatory than that currently portrayed in the literature for prion disease, and more
486 akin to other protein-misfolding diseases, notably Alzheimer's disease, in which microglia
487 are observed as expressing a repertoire of pro-inflammatory cytokines including *Tnfa*, *Il1b*
488 and *Il6* (93-95). The increased expression of cytokines *Il1b*, *Tnfa* and *Csf1*, but not *Il6* in this
489 dataset suggests an activation profile that is specific to prion disease and likely also unique
490 to the in-vivo environment since co-cultures of microglia and neurons in the presence of
491 $PrP^{106\text{-}126}$ induces a stereotypic response with CD14 mediated detection of damaged neurons
492 and increased expression of Il6 (96). This matches the stereotypic neurotoxic response
493 observed in co-cultures of neurons in the presence of LPS activated microglia (97).
494
495 Our study demonstrated that genes up-regulated throughout the disease process, are
496 expressed predominately by microglia. A disease specific highly pro-inflammatory signature
497 was observed in addition to an up-regulation of genes associated with metabolism and
498 respiratory stress. This study strongly supports the growing recognition of the important
499 contribution of microglia to a chronic neurodegenerative disease process. Protein misfolding
500 diseases typically have a very long pre-clinical phase in which there is a steady and
501 progressive increase in misfolded protein deposition, neuroinflammation and synaptopathy
502 as the disease progresses. Thus an understanding of the contributors to this pre-clinical

Journal of Virology

Accepted Manuscript Posted Online

Journal of Virology

JVI

Journal of Virology

503 phase provides opportunities for devising early intervention strategies to limit the pathology
504 before damage becomes irreversible

Funding Information

505 This study was funded by DTA studentship from the BBSRC. The funders had no role in
506 study design, data collection and interpretation

Acknowledgements

We would like to acknowledge the extensive support and expertise of Mrs Aileen Boyle, Mrs Gillian McGregor, Ms Dawn Drummond and Mrs Sandra Mack for pathology services, Mrs Rebecca Hogan for animal care, Mr Bob Fleming and Dr Deborah Brown for assistance with bioimaging and to Ms Lynesay McKay for assistance with Miltenyi Biotec equipment.

GEO accession number: GSE72039

507

508 ***References***

509 1. **Williams AE, van Dam AM, Man-A-Hing WKH, Berkenbosch F, Eikelenboom P, Fraser H.**
510 1994. Cytokines, prostaglandins and lipocortin-1 are present in the brains of scrapie-infected
511 mice. Brain Research **654:**200-206.
512 2. **Betmouni S, Perry VH, Gordon JL.** 1996. Evidence for an early inflammatory response in the
513 central nervous system of mice with scrapie. Neuroscience **74:**1-5.
514 3. **Ye X, Scallet AC, Kascsak RJ, Carp RI.** 1998. Astrocytosis and amyloid deposition in scrapie-
515 infected hamsters. Brain Res **809:**277-287.
516 4. **Jebelli J, Su W, Hopkins S, Pocock J, Garden GA.** 2015. Glia: guardians, gluttons, or guides
517 for the maintenance of neuronal connectivity? Annals of the New York Academy of
518 Sciences:n/a-n/a.
519 5. **Williams A, Lucassen PJ, Ritchie D, Bruce M.** 1997. PrP Deposition, Microglial Activation, and
520 Neuronal Apoptosis in Murine Scrapie. Experimental Neurology **144:**433-438.

Accepted Manuscript Posted Online

Journal of Virology

JVI

Journal of Virology

521 6. **Baker CA, Lu ZY, Zaitsev I, Manuelidis L.** 1999. Microglial Activation Varies in Different
522 Models of Creutzfeldt-Jakob Disease. J. Virol. **73:**5089-5097.
523 7. **Cunningham C, Boche D, Perry VH.** 2002. Transforming growth factor β1, the dominant
524 cytokine in murine prion disease: influence on inflammatory cytokine synthesis and
525 alteration of vascular extracellular matrix. Neuropathol Appl Neurobiol **28:**107-119.
526 8. **Lawson LJ, Perry VH, Dri P, Gordon S.** 1990. Heterogeneity in the distribution and
527 morphology of microglia in the normal adult mouse brain. Neuroscience **39:**151-170.
528 9. **Hart AD, Wyttenbach A, Perry VH, Teeling JL.** 2012. Age related changes in microglial
529 phenotype vary between CNS regions: grey versus white matter differences. Brain, behavior,
530 and immunity **26:**754-765.
531 10. **Nimmerjahn A, Kirchhoff F, Helmchen F.** 2005. Resting Microglial Cells Are Highly Dynamic
532 Surveillants of Brain Parenchyma in Vivo. Science **308:**1314-1318.
533 11. **Davalos D, Grutzendler J, Yang G, Kim JV, Zuo Y, Jung S, Littman DR, Dustin ML, Gan WB.**
534 2005. ATP mediates rapid microglial response to local brain injury in vivo. Nature
535 neuroscience **8:**752-758.
536 12. **Kozai TD, Vazquez AL, Weaver CL, Kim SG, Cui XT.** 2012. In vivo two-photon microscopy
537 reveals immediate microglial reaction to implantation of microelectrode through extension
538 of processes. Journal of neural engineering **9:**066001.
539 13. **Perry VH, Nicoll JAR, Holmes C.** 2010. Microglia in neurodegenerative disease. Nature
540 Reviews Neurology **6:**193-201.
541 14. **Mosser DM, Edwards JP.** 2008. Exploring the full spectrum of macrophage activation. Nat
542 Rev Immunol **8:**958-969.
543 15. **Xue J, Schmidt SV, Sander J, Draffehn A, Krebs W, Quester I, De Nardo D, Gohel TD, Emde**
544 **M, Schmidleithner L, Ganesan H, Nino-Castro A, Mallmann MR, Labzin L, Theis H, Kraut M,**
545 **Beyer M, Latz E, Freeman TC, Ulas T, Schultze JL.** 2014. Transcriptome-based network
546 analysis reveals a spectrum model of human macrophage activation. Immunity **40:**274-288.
547 16. **Martinez FO, Sica A, Mantovani A, Locati M.** 2008. Macrophage activation and polarization.
548 Frontiers in bioscience : a journal and virtual library **13:**453-461.
549 17. **Palin K, Cunningham C, Forse P, Perry VH, Platt N.** 2008. Systemic inflammation switches
550 the inflammatory cytokine profile in CNS Wallerian degeneration. Neurobiology of disease
551 **30:**19-29.
552 18. **Murray CL, Skelly DT, Cunningham C.** 2011. Exacerbation of CNS inflammation and
553 neurodegeneration by systemic LPS treatment is independent of circulating IL-1beta and IL-
554 6. Journal of neuroinflammation **8:**50.
555 19. **Field R, Campion S, Warren C, Murray C, Cunningham C.** 2010. Systemic challenge with the
556 TLR3 agonist poly I:C induces amplified IFNalpha/beta and IL-1beta responses in the
557 diseased brain and exacerbates chronic neurodegeneration. Brain, behavior, and immunity
558 **24:**996-1007.
559 20. **Thomson CA, McColl A, Cavanagh J, Graham GJ.** 2014. Peripheral inflammation is associated
560 with remote global gene expression changes in the brain. Journal of neuroinflammation
561 **11:**73.
562 21. **Lunnon K, Teeling JL, Tutt AL, Cragg MS, Glennie MJ, Perry VH.** 2011. Systemic inflammation
563 modulates Fc receptor expression on microglia during chronic neurodegeneration. J
564 Immunol **186:**7215-7224.
565 22. **Combrinck MI, Perry VH, Cunningham C.** 2002. Peripheral infection evokes exaggerated
566 sickness behaviour in pre-clinical murine prion disease. Neuroscience **112:**7-11.
567 23. **Perry VH, Teeling J.** 2013. Microglia and macrophages of the central nervous system: the
568 contribution of microglia priming and systemic inflammation to chronic neurodegeneration.
569 Seminars in immunopathology.
570 24. **Saura J.** 2007. Microglial cells in astroglial cultures: a cautionary note. Journal of
571 neuroinflammation **4:**26.

Accepted Manuscript Posted Online
Journal of Virology
JVI

572 25. **Lee M, Schwab C, McGeer PL.** 2011. Astrocytes are GABAergic cells that modulate microglial
573 activity. Glia **59:**152-165.
574 26. **Cardona AE, Pioro EP, Sasse ME, Kostenko V, Cardona SM, Dijkstra IM, Huang D, Kidd G,**
575 **Dombrowski S, Dutta R, Lee JC, Cook DN, Jung S, Lira SA, Littman DR, Ransohoff RM.** 2006.
576 Control of microglial neurotoxicity by the fractalkine receptor. Nature neuroscience **9:**917-
577 924.
578 27. **Boche D, Cunningham C, Docagne F, Scott H, Perry VH.** 2006. TGF[beta]1 regulates the
579 inflammatory response during chronic neurodegeneration. Neurobiology of disease **22:**638-
580 650.
581 28. **Hwang D, Lee IY, Yoo H, Gehlenborg N, Cho J-H, Petritis B, Baxter D, Pitstick R, Young R,**
582 **Spicer D, Price ND, Hohmann JG, DeArmond SJ, Carlson GA, Hood LE.** 2009. A systems
583 approach to prion disease. Mol Syst Biol **5:**252.
584 29. **Kauffmann A, Gentleman R, Huber W.** 2009. arrayQualityMetrics--a bioconductor package
585 for quality assessment of microarray data. Bioinformatics (Oxford, England) **25:**415-416.
586 30. **Irizarry RA, Hobbs B, Collin F, Beazer-Barclay YD, Antonellis KJ, Scherf U, Speed TP.** 2003.
587 Exploration, normalization, and summaries of high density oligonucleotide array probe level
588 data. Biostatistics (Oxford, England) **4:**249-264.
589 31. **Freeman TC, Goldovsky L, Brosch M, van Dongen S, Mazière P, Grocock RJ, Freilich S,**
590 **Thornton J, Enright AJ.** 2007. Construction, visualisation, and clustering of transcription
591 networks from microarray expression data. PLoS Computational Biology **3:**2032-2042.
592 32. **Dongen V.** 2000. Performance criteria for graph clustering and Markov cluster experiments.
593 CWI (Centre for Mathematics and Computer Science)**:**INS-R0012.
594 33. **Wu C, Orozco C, Boyer J, Leglise M, Goodale J, Batalov S, Hodge CL, Haase J, Janes J, Huss**
595 **JW, 3rd, Su AI.** 2009. BioGPS: an extensible and customizable portal for querying and
596 organizing gene annotation resources. Genome Biol **10:**2009-2010.
597 34. **Su AI, Cooke MP, Ching KA, Hakak Y, Walker JR, Wiltshire T, Orth AP, Vega RG, Sapinoso**
598 **LM, Moqrich A, Patapoutian A, Hampton GM, Schultz PG, Hogenesch JB.** 2002. Large-scale
599 analysis of the human and mouse transcriptomes. Proc Natl Acad Sci U S A **99:**4465-4470.
600 35. **Doyle JP, Dougherty JD, Heiman M, Schmidt EF, Stevens TR, Ma G, Bupp S, Shrestha P,**
601 **Shah RD, Doughty ML, Gong S, Greengard P, Heintz N.** 2008. Application of a translational
602 profiling approach for the comparative analysis of CNS cell types. Cell **135:**749-762.
603 36. **Heiman M, Schaefer A, Gong S, Peterson JD, Day M, Ramsey KE, Suarez-Farinas M, Schwarz**
604 **C, Stephan DA, Surmeier DJ, Greengard P, Heintz N.** 2008. A translational profiling approach
605 for the molecular characterization of CNS cell types. Cell **135:**738-748.
606 37. **Lattin JE, Schroder K, Su AI, Walker JR, Zhang J, Wiltshire T, Saijo K, Glass CK, Hume DA,**
607 **Kellie S, Sweet MJ.** 2008. Expression analysis of G Protein-Coupled Receptors in mouse
608 macrophages. Immunome Res **4:**1745-7580.
609 38. **Sasmono RT, Oceandy D, Pollard JW, Tong W, Pavli P, Wainwright BJ, Ostrowski MC, Himes**
610 **SR, Hume DA.** 2003. A macrophage colony-stimulating factor receptor-green fluorescent
611 protein transgene is expressed throughout the mononuclear phagocyte system of the
612 mouse. Blood **101:**1155-1163.
613 39. **Dickinson AG, Meikle VM, Fraser H.** 1968. Identification of a gene which controls the
614 incubation period of some strains of scrapie agent in mice. J Comp Pathol **78:**293-299.
615 40. **Fraser H, Dickinson AG.** 1967. Distribution of experimentally induced scrapie lesions in the
616 brain. NATURE **216:**1310-1311.
617 41. **Korth C, Stierli B, Streit P, Moser M, Schaller O, Fischer R, Schulz-Schaeffer W, Kretzschmar**
618 **H, Raeber A, Braun U, Ehrensperger F, Hornemann S, Glockshuber R, Riek R, Billeter M,**
619 **Wuthrich K, Oesch B.** 1997. Prion (PrPSc)-specific epitope defined by a monoclonal antibody.
620 Nature **390:**74-77.
621 42. **Cancellotti E, Bradford BM, Tuzi NL, Hickey RD, Brown D, Brown KL, Barron RM, Kisielewski**
622 **D, Piccardo P, Manson JC.** 2010. Glycosylation of PrP^C determines timing of neuroinvasion

Journal of Virology

Accepted Manuscript Posted Online

623 and targeting in the brain following transmissible spongiform encephalopathy infection by a
624 peripheral route. J Virol **84:**3464-3475.
625 43. **Giese A, Brown DR, Groschup MH, Feldmann C, Haist I, Kretzschmar HA.** 1998. Role of
626 Microglia in Neuronal Cell Death in Prion Disease. Brain Pathology **8:**449-457.
627 44. **Bruce ME.** 1993. Scrapie strain variation and mutation. Br Med Bull **49:**822-838.
628 45. **McGeer PL, Kawamata T, Walker DG, Akiyama H, Tooyama I, McGeer EG.** 1993. Microglia in
629 degenerative neurological disease. Glia **7:**84-92.
630 46. **Ginhoux F, Greter M, Leboeuf M, Nandi S, See P, Gokhan S, Mehler MF, Conway SJ, Ng LG,**
631 **Stanley ER, Samokhvalov IM, Merad M.** 2010. Fate mapping analysis reveals that adult
632 microglia derive from primitive macrophages. Science **330:**841-845.
633 47. **Berriz GF, King OD, Bryant B, Sander C, Roth FP.** 2003. Characterizing gene sets with
634 FuncAssociate. Bioinformatics **19:**2502-2504.
635 48. **Akira S, Takeda K.** 2004. Toll-like receptor signalling. Nat Rev Immunol **4:**499-511.
636 49. **Croft D, Mundo AF, Haw R, Milacic M, Weiser J, Wu G, Caudy M, Garapati P, Gillespie M,**
637 **Kamdar MR, Jassal B, Jupe S, Matthews L, May B, Palatnik S, Rothfels K, Shamovsky V,**
638 **Song H, Williams M, Birney E, Hermjakob H, Stein L, D'Eustachio P.** 2014. The Reactome
639 pathway knowledgebase. Nucleic Acids Res **42:**D472-477.
640 50. **Brooks GA, Dubouchaud H, Brown M, Sicurello JP, Butz CE.** 1999. Role of mitochondrial
641 lactate dehydrogenase and lactate oxidation in the intracellular lactate shuttle. Proc Natl
642 Acad Sci U S A **96:**1129-1134.
643 51. **Ame JC, Spenlehauer C, de Murcia G.** 2004. The PARP superfamily. BioEssays : news and
644 reviews in molecular, cellular and developmental biology **26:**882-893.
645 52. **Mehrotra P, Riley JP, Patel R, Li F, Voss L, Goenka S.** 2011. PARP-14 functions as a
646 transcriptional switch for Stat6-dependent gene activation. The Journal of biological
647 chemistry **286:**1767-1776.
648 53. **Mantovani A, Sica A, Sozzani S, Allavena P, Vecchi A, Locati M.** 2004. The chemokine
649 system in diverse forms of macrophage activation and polarization. Trends in immunology
650 **25:**677-686.
651 54. **Samuel D, Kroner A.** 2011. Repertoire of microglial and macrophage responses after spinal
652 cord injury. Nat Rev Neurosci **12:**388-399.
653 55. **Elishmereni M, Levi-Schaffer F.** 2011. CD48: A co-stimulatory receptor of immunity. The
654 international journal of biochemistry & cell biology **43:**25-28.
655 56. **Dantzer R.** 2004. Cytokine-induced sickness behaviour: a neuroimmune response to
656 activation of innate immunity. European Journal of Pharmacology **500:**399-411.
657 57. **Lemstra AW, Groen in't Woud JCM, Hoozemans JJM, van Haastert ES, Rozemuller AJM,**
658 **Eikelenboom P, van Gool WA.** 2007. Microglia activation in sepsis: a case-control study.
659 Journal of neuroinflammation **4:**4-4.
660 58. **Quan N, Banks WA.** 2007. Brain-immune communication pathways. Brain, behavior, and
661 immunity **21:**727-735.
662 59. **Newsom DM, Liggitt HD, O'Rourke K, Zhuang D, Schneider DA, Harrington RD.** 2011.
663 Cytokine antibody array analysis in brain and periphery of scrapie-infected Tg338 mice.
664 Comparative immunology, microbiology and infectious diseases **34:**387-397.
665 60. **Cunningham C, Wilcockson DC, Boche D, Perry VH.** 2005. Comparison of Inflammatory and
666 Acute-Phase Responses in the Brain and Peripheral Organs of the ME7 Model of Prion
667 Disease. J Virol **79:**5174-5184.
668 61. **Walsh DTP, Betmouni SD, Perry VHD.** 2001. Absence of Detectable IL-1[beta] Production in
669 Murine Prion Disease: A Model of Chronic Neurodegeneration. [Article]. Journal of
670 neuropathology and experimental neurology **60:**173-182.
671 62. **Romano M, Sironi M, Toniatti C, Polentarutti N, Fruscella P, Ghezzi P, Faggioni R, Luini W,**
672 **van Hinsbergh V, Sozzani S, Bussolino F, Poli V, Ciliberto G, Mantovani A.** 1997. Role of IL-6

JVI Journal of Virology

Accepted Manuscript Posted Online

Journal of Virology

JVI

673 and Its Soluble Receptor in Induction of Chemokines and Leukocyte Recruitment. Immunity
674 **6:**315-325.
675 63. **Schmitz J, Owyang A, Oldham E, Song Y, Murphy E, McClanahan TK, Zurawski G, Moshrefi**
676 **M, Qin J, Li X, Gorman DM, Bazan JF, Kastelein RA.** 2005. IL-33, an interleukin-1-like
677 cytokine that signals via the IL-1 receptor-related protein ST2 and induces T helper type 2-
678 associated cytokines. Immunity **23:**479-490.
679 64. **Kakkar R, Hei H, Dobner S, Lee RT.** 2012. Interleukin 33 as a mechanically responsive
680 cytokine secreted by living cells. The Journal of biological chemistry **287:**6941-6948.
681 65. **Arenzana-Seisdedos F, Thompson J, Rodriguez MS, Bachelerie F, Thomas D, Hay RT.** 1995.
682 Inducible nuclear expression of newly synthesized I kappa B alpha negatively regulates DNA-
683 binding and transcriptional activities of NF-kappa B. Molecular and cellular biology **15:**2689-
684 2696.
685 66. **Baker CA, Manuelidis L.** 2003. Unique inflammatory RNA profiles of microglia in Creutzfeldt–
686 Jakob disease. Proc Natl Acad Sci U S A **100:**675-679.
687 67. **Abutbul S, Shapiro J, Szaingurten-Solodkin I, Levy N, Carmy Y, Baron R, Jung S, Monsonego**
688 **A.** 2012. TGF-beta signaling through SMAD2/3 induces the quiescent microglial phenotype
689 within the CNS environment. Glia **60:**1160-1171.
690 68. **Fadok VA, Bratton DL, Konowal A, Freed PW, Westcott JY, Henson PM.** 1998. Macrophages
691 that have ingested apoptotic cells in vitro inhibit proinflammatory cytokine production
692 through autocrine/paracrine mechanisms involving TGF-beta, PGE2, and PAF. The Journal of
693 clinical investigation **101:**890-898.
694 69. **Lodge PA, Sriram S.** 1996. Regulation of microglial activation by TGF-beta, IL-10, and CSF-1. J
695 Leukoc Biol **60:**502-508.
696 70. **Butovsky O, Jedrychowski MP, Moore CS, Cialic R, Lanser AJ, Gabriely G, Koeglsperger T,**
697 **Dake B, Wu PM, Doykan CE, Fanek Z, Liu L, Chen Z, Rothstein JD, Ransohoff RM, Gygi SP,**
698 **Antel JP, Weiner HL.** 2014. Identification of a unique TGF-beta-dependent molecular and
699 functional signature in microglia. Nature neuroscience **17:**131-143.
700 71. **Heldin CH, Miyazono K, ten Dijke P.** 1997. TGF-beta signalling from cell membrane to
701 nucleus through SMAD proteins. Nature **390:**465-471.
702 72. **Tsukazaki T, Chiang TA, Davison AF, Attisano L, Wrana JL.** 1998. SARA, a FYVE domain
703 protein that recruits Smad2 to the TGFbeta receptor. Cell **95:**779-791.
704 73. **Inui M, Manfrin A, Mamidi A, Martello G, Morsut L, Soligo S, Enzo E, Moro S, Polo S,**
705 **Dupont S, Cordenonsi M, Piccolo S.** 2011. USP15 is a deubiquitylating enzyme for receptor-
706 activated SMADs. Nature cell biology **13:**1368-1375.
707 74. **Kastin AJ, Akerstrom V, Pan W.** 2003. Circulating TGF-beta1 does not cross the intact blood-
708 brain barrier. Journal of molecular neuroscience : MN **21:**43-48.
709 75. **Dohgu S, Yamauchi A, Takata F, Naito M, Tsuruo T, Higuchi S, Sawada Y, Kataoka Y.** 2004.
710 Transforming growth factor-beta1 upregulates the tight junction and P-glycoprotein of brain
711 microvascular endothelial cells. Cellular and molecular neurobiology **24:**491-497.
712 76. **Siskova Z, Tremblay ME.** 2013. Microglia and synapse: interactions in health and
713 neurodegeneration. Neural plasticity **2013:**425845.
714 77. **Tremblay M-È, Lowery RL, Majewska AK.** 2010. Microglial interactions with synapses are
715 modulated by visual experience. PLoS Biology **8:**e1000527.
716 78. **Chen Z, Jalabi W, Hu W, Park HJ, Gale JT, Kidd GJ, Bernatowicz R, Gossman ZC, Chen JT,**
717 **Dutta R, Trapp BD.** 2014. Microglial displacement of inhibitory synapses provides
718 neuroprotection in the adult brain. Nature communications **5:**4486.
719 79. **Ji K, Akgul G, Wollmuth LP, Tsirka SE.** 2013. Microglia Actively Regulate the Number of
720 Functional Synapses. PLoS One **8:**e56293.
721 80. **Miyamoto A, Wake H, Moorhouse AJ, Nabekura J.** 2013. Microglia and synapse
722 interactions: fine tuning neural circuits and candidate molecules. Frontiers In Cellular
723 Neuroscience **7:**1-6.

Accepted Manuscript Posted Online
Journal of Virology
JVI
Journal of Virology

724 81. **Vukovic J, Colditz MJ, Blackmore DG, Ruitenberg MJ, Bartlett PF.** 2012. Microglia modulate
725 hippocampal neural precursor activity in response to exercise and aging. The Journal of
726 neuroscience : the official journal of the Society for Neuroscience **32:**6435-6443.
727 82. **Schafer DP, Lehrman EK, Stevens B.** 2013. The "quad-partite" synapse: Microglia-synapse
728 interactions in the developing and mature CNS. Glia **61:**24-36.
729 83. **Sogn C, Puchades M, Gundersen V.** 2013. Rare contacts between synapses and microglial
730 processes containing high levels of Iba1 and actin - a postembedding immunogold study in
731 the healthy rat brain. European Journal of Neuroscience**:**2030-2040.
732 84. **Bate C, Reid S, Williams A.** 2001. Killing of prion-damaged neurones by microglia.
733 Neuroreport **12:**2589-2594.
734 85. **Franchi L, Eigenbrod T, Munoz-Planillo R, Nunez G.** 2009. The inflammasome: a caspase-1-
735 activation platform that regulates immune responses and disease pathogenesis. Nat
736 Immunol **10:**241-247.
737 86. **Martinon F, Tschopp J.** 2007. Inflammatory caspases and inflammasomes: master switches
738 of inflammation. Cell Death Differ **14:**10-22.
739 87. **Sollberger G, Strittmatter GE, Kistowska M, French LE, Beer HD.** 2012. Caspase-4 is required
740 for activation of inflammasomes. J Immunol **188:**1992-2000.
741 88. **Bai Y, Zhu Z, Gao Z, Kong Y.** 2014. TLR2 signaling directs NO-dependent MMP-9 induction in
742 mouse microglia. Neuroscience letters **571:**5-10.
743 89. **Minghetti l.** 2004. Cyclooxygenase-2 (COX-2) in Inflammatory and Degenerative Brain
744 Diseases. Journal of neuropathology and experimental neurology **63:**901-910.
745 90. **Minghetti L, Pocchiari M.** 2007. Cyclooxygenase-2, prostaglandin E2, and microglial
746 activation in prion diseases. International review of neurobiology **82:**265-275.
747 91. **Walsh DT, Perry VH, Minghetti L.** 2000. Cyclooxygenase-2 is highly expressed in microglial-
748 like cells in a murine model of prion disease. Glia **29:**392-396.
749 92. **Vane JR.** 1971. Inhibition of prostaglandin synthesis as a mechanism of action for aspirin-like
750 drugs. Nature: New biology **231:**232-235.
751 93. **Bhaskar K, Maphis N, Xu G, Varvel NH, Kokiko-Cochran ON, Weick JP, Staugaitis SM,**
752 **Cardona A, Ransohoff RM, Herrup K, Lamb BT.** 2014. Microglial derived tumor necrosis
753 factor-alpha drives Alzheimer's disease-related neuronal cell cycle events. Neurobiology of
754 disease **62:**273-285.
755 94. **Griffin WS, Sheng JG, Roberts GW, Mrak RE.** 1995. Interleukin-1 expression in different
756 plaque types in Alzheimer's disease: significance in plaque evolution. Journal of
757 neuropathology and experimental neurology **54:**276-281.
758 95. **Tarkowski E, Blennow K, Wallin A, Tarkowski A.** 1999. Intracerebral production of tumor
759 necrosis factor-alpha, a local neuroprotective agent, in Alzheimer disease and vascular
760 dementia. Journal of clinical immunology **19:**223-230.
761 96. **Bate C, Boshuizen R, Williams A.** 2005. Microglial cells kill prion-damaged neurons in vitro
762 by a CD14-dependent process. J Neuroimmunol **170:**62-70.
763 97. **Chao CC, Hu S, Molitor TW, Shaskan EG, Peterson PK.** 1992. Activated microglia mediate
764 neuronal cell injury via a nitric oxide mechanism. J Immunol **149:**2736-2741.
765

766

767

Accepted Manuscript Posted Online
Journal of Virology
JVI
Journal of Virology

768 **Figure Legends**

769 ***Figure 1 -* BioLayout *Express^{3D} generated transcript -to-transcript network graph of***
770 ***selected genes of interest.***

771 **A:** The list of 492 genes of interest with an expression pattern indicative of disease
772 association were organised into 2 main clusters within BioLayout *Express*^{3D} by MCL. The
773 green cluster comprising 410 nodes was joined by 29,339 edges indicating a high degree of
774 co-expression between genes. The smaller purple cluster comprised 67 nodes and 1453
775 edges. **B:** The disease associated gene expression signatures of both clusters, displayed as a
776 mean expression profile for each strain, revealed an up-regulation at approx. 50% of
777 incubation period. The profile was similar for all genes in all mouse/prion combinations.
778 The smaller purple cluster was expressed highest in BL6 strains resulting in the formation of
779 a separate cluster. Error bars equate to ± SE. Grey triangles on X-axis indicate the incubation
780 period between the point of inoculation to cull, some mouse/TSE strains leading to
781 pathology and death faster than others.
782

783 **Figure 2 -** ***Cross reference of the 492 disease associated genes with co-normalised external***
784 ***datasets within* BioLayout *Express^{3D}.***

785 Within BioLayout E*xpress*^{3D} each gene of interest was classed and coloured as a specific cell
786 type. Note how the previously determined MCL clusters are both dominated by myeloid
787 derived genes (green). Genes associated with myeloid were divided into two groups based
788 on sole association with myeloid cell types or in which sole origin could not be determined.
789 Sole myeloid origin comprised 318 genes or 64% of the gene set. A total of 146 genes were
790 associated with multiple cell types found within the CNS. Here a myeloid component was

Accepted Manuscript Posted Online

Journal of Virology

JVI

791 still observed as strongly associated with the group. Genes assigned to astrocytes,
792 oligodendrocytes and neurons were each represented by <20 genes.
793
794
795 ***Figure 3 - PrP Deposition and Microglia Activation Assessed by immunohistochemistry***
796 Microglia activation was observed in the same areas as PrP deposition. **A/B:** Earliest
797 accumulation of PrP (6H4) is at 150 dpi in the Medulla. Microglia can be seen **C/D:** as
798 accumulating in the same areas of deposition. **E/F:** Normal Microglia in the thalamus and
799 medulla respectively of mice challenged with normal brain demonstrate a ramified
800 appearance and greater separation at ~ 50 µm. All images representative. Scale bars
801 equate to 100 µm.
802
803
804 ***Figure 4 - Software determined quantification of EGFP expressing microglia in 79A infected***
805 ***BALB/cJ$^{Fms\text{-}EGFP/-}$ mice.***

806 **A:** Quantification of regional microglia cell number in BALB/cJ$^{Fms\text{-}EGFP/-}$ mice following i.p.
807 challenge with 79A at 100, 150 and 200 dpi. EGFP expressing cells were counting using
808 ImageJ particle analysis function on x10 magnification 25µm Z-stack compiled images each
809 comprising 50 optical slices. Microglia density increases in the medulla by ~ 50% at 150 dpi
810 whereupon numbers remain constant in this region as PrP deposition spreads anteriorly. By
811 200 dpi microglia density in the thalamus has increased by ~ 100%. **B:** EGFP expressing
812 microglia in the thalamus of BALB/cJ$^{Fms\text{-}EGFP/-}$ mice following i.p. challenge with 79A at 150
813 and 200 dpi. No difference in the number of EGFP expressing cells was observed in the

Journal of Virology

Accepted Manuscript Posted Online

814 thalamus until 200 dpi when a concentration of reactive microglia spaced less than 25 µm
815 was observed. Before 200 dpi microglia were observed in all animals as spaced at 50 - 100
816 µm and adopt a normal ramified morphology. Scale bars equate to 200 µm. Inset scale bars
817 equate to 20 µm. **C:** At 200 dpi, microglia present with an engorged central body and
818 shortened processes conferring a significant reduction in radius. D: Euclidean distance
819 mapping affords a highly sensitive quantification of cell complexity encompassing both cell
820 body size and process branching. The reduction in cell radius at 200 dpi is reflected in a
821 mean Euclidean distance increase of 1 µm. Distance mapping also detailed a slightly less
822 complex cell type in the NBr animals. **E:** High Resolution image analysis of microglia density
823 per 0.05 mm^2 in the thalamus at 200 dpi revealed an increase of ~ 100%. † Comprises mean
824 for all NBr inoculated BALB/cJ$^{Fms\text{-}EGFP/-}$ mice at all serial investigation time points. ‡ Mean
825 statistical value determined using *t*-Test assuming variances determined by *f*-Test. *NS* = Not
826 Significant. A, C-E: error bars equate to ± SE.
827

828 ***Figure 5 - Purity of isolated microglia was confirmed to be high and extracted RNA was***
829 ***confirmed to be of workable quality.***

830 **A:** FACS sample analysis of CD11b microbead purified microglia stained with, and positive
831 for, CD11b-PE & CD45-APC demonstrate a high purity. **B:** Isotope control and **C**: negative
832 control show no non-specific binding or auto-fluorescence respectively. **D:** Cell viability was
833 confirmed using SYTOX® live-dead stain. Inset: Isolated cells are EGFP positive. **E:** Plot of the
834 mean expression profile of twenty genes known to be expressed in a cell-specific manner.
835 The first five are known microglial expressed genes, the remainder are expressed in other
836 brain cell types. This demonstrates that the expression of non-microglia genes in isolated

Journal of Virology JVI Journal of Virology

Accepted Manuscript Posted Online

837 microglial populations is negligible, suggesting a relatively pure microglial population. Error
838 bars equate to ± SE.
839
840 ***Figure 6* - BioLayout *Express^{3D}* *analysis of isolated microglia gene expression.***
841 **A:** Average expression profile of the 2 large clusters produced within BioLayout *Express*^{3D} by
842 the 741 genes that demonstrate a differential expression in response to disease. All genes
843 yielded an increase in expression with a large escalation at 200 dpi in 79A infected mice.
844 Error bars equate to ± SE. **B:** Global microarray sample-to-sample transposed BioLayout
845 *Express*^{3D} graph of the 741 identified genes of interest. Prion infected and uninfected pre-
846 200 dpi arrays are highly correlated and organised into one component. Displaying high
847 inter-correlation but lower correlation with the rest of the population are the arrays for the
848 200 dpi infected group. Note: nodes have been coloured only for clarity and are not
849 indicative of MCL clustering.
850
851 ***Figure 7 - Ontological analysis of the microglia activation signature within the 741 genes***
852 ***of interest.***
853 **A:** GO enrichment terms determined from the identified 741 differentially expressed genes
854 using FuncAssociate 2.0 revealed protein translation, respiration, cellular stress and
855 components of the myeloid immune system to be significantly represented. All terms have
856 a *P*-value of considerably less than 0.001. **B:** Regulated disease-associated genes allocated
857 by function. Using the Ensembl Biomart database the majority of the regulated genes were
858 ascribed to metabolism and homeostasis. Genes associated with immune system, for which
859 differentiation has been included, comprise only a fifth. This highlights the power of a signal

Journal of Virology
JVI
Journal of Virology

Accepted Manuscript Posted Online
Journal of Virology
JVI

860 cell isolation in correctly determining the association of metabolic genes with a specific cell
861 type. **C**: Expression of inflammatory cytokines and transcription factors associated with the
862 regulation of activation phenotype of microglia. Strong increase in expression of *Tnfa* and
863 *Il1b,* but not cytokines associated with recruitment and escalation toward acquired
864 immunity imply a disease-specific signature. **D:** Nominal and unchanged expression of
865 *Tgfb1* is matched by a lack of expression of downstream transcripts mediated by TGFB1
866 activity. C-D error bars equate to ± SE.
867
868 ***Figure 8 - Genes of interest associated with metabolism and homeostasis.***
869 A considerable number of genes with an increase in expression are associated with protein
870 translation and processing. The increased metabolic load is reflected in the increase in
871 expression of genes associated with energy production.
872
873 ***Figure 9 - Genes of interest associated with immune activation and cell-to-cell signalling.***
874 Genes have been grouped by both function and cellular location. The signature is one of
875 robust pro-inflammatory innate immune activation.
876
877

Journal of Virology

Accepted Manuscript Posted Online
Journal of Virology
JVI
Journal of Virology

Figure 1

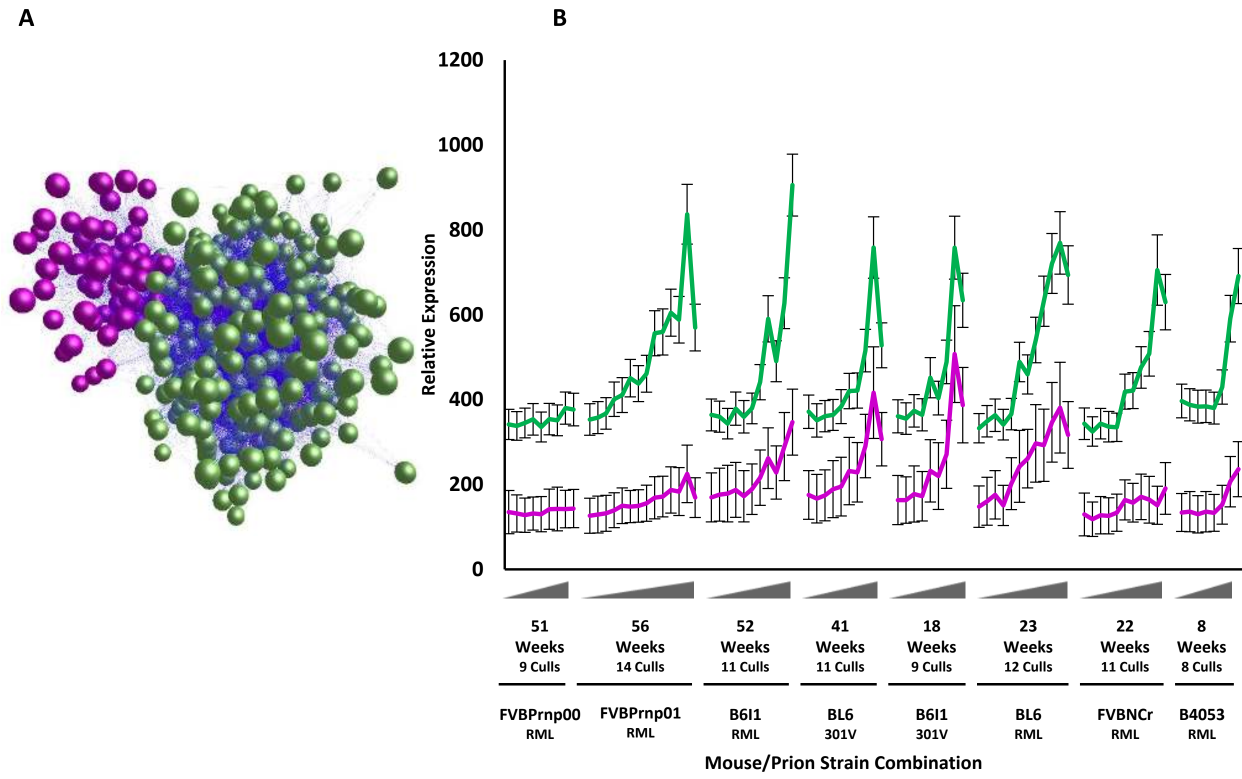

Accepted Manuscript Posted Online
JVI
Journal of Virology
Journal of Virology

Figure 2

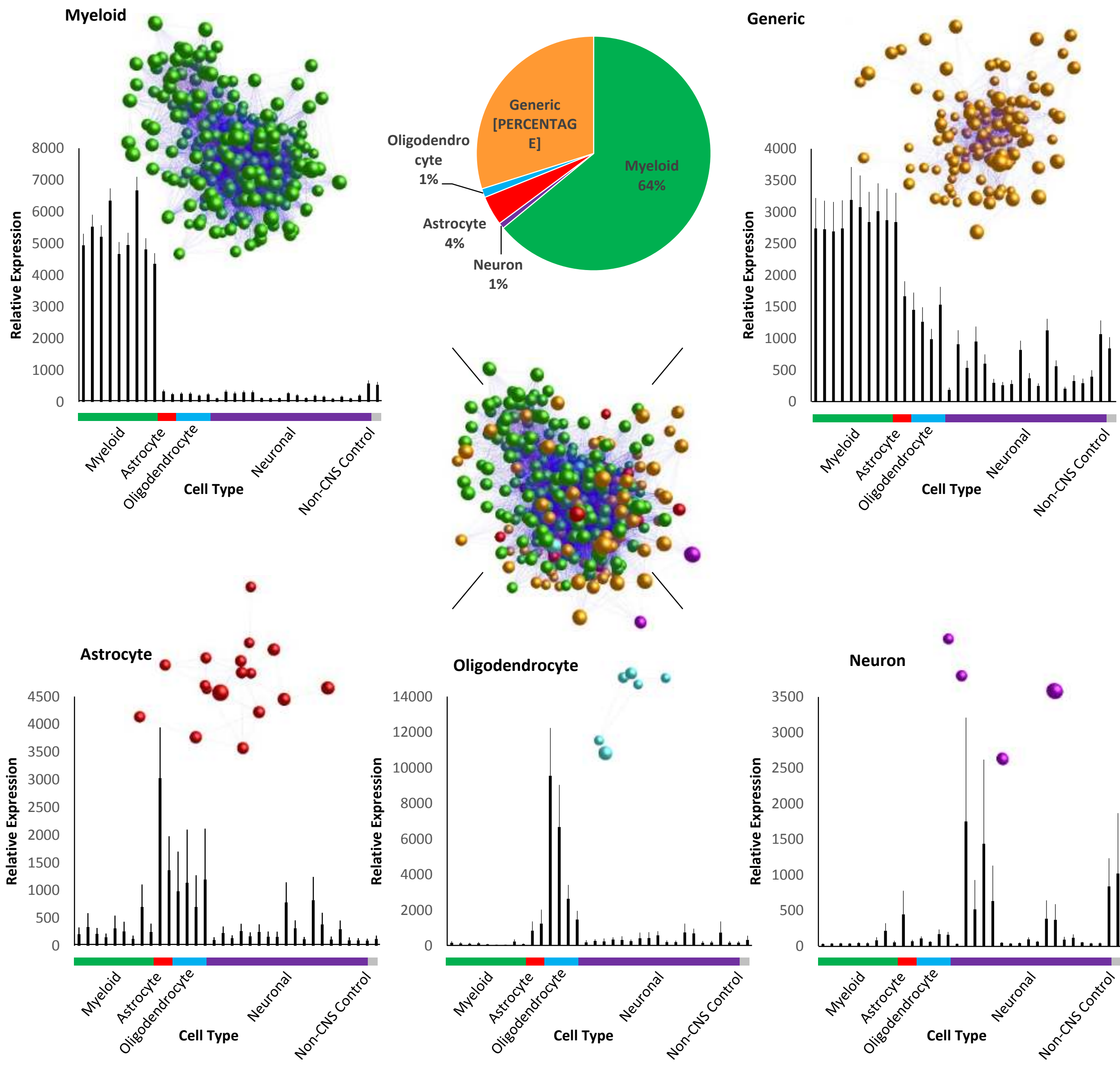

Accepted Manuscript Posted Online

Journal of Virology

JVI

Journal of Virology

Figure 3

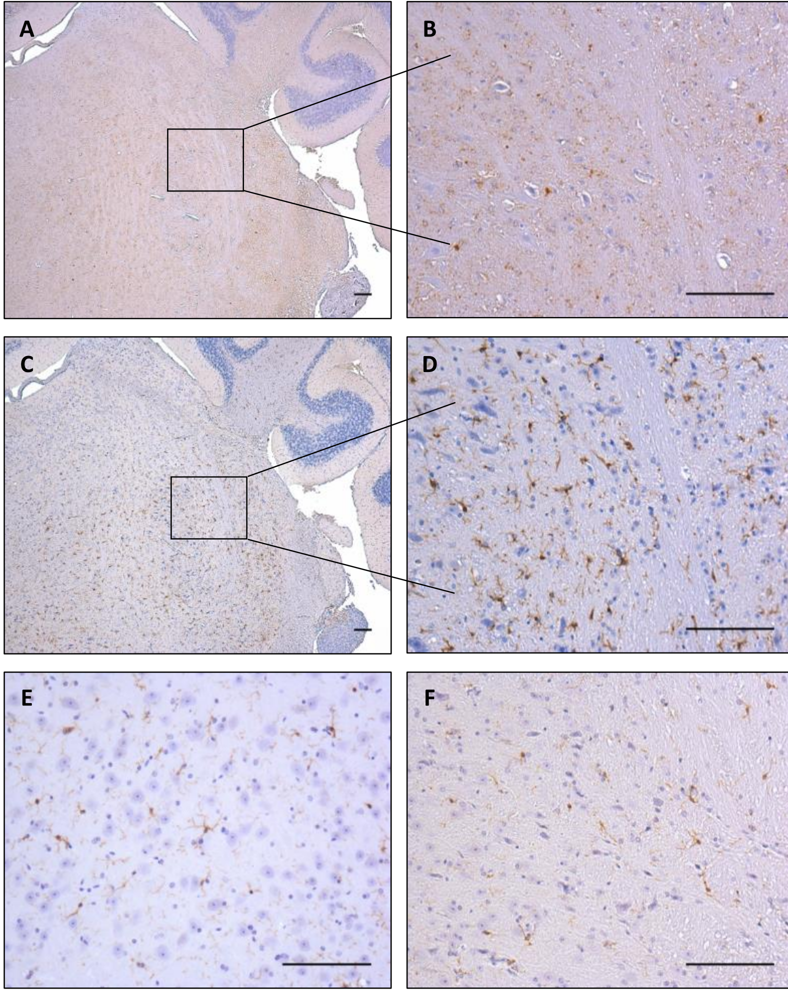

Accepted Manuscript Posted Online

Figure 4

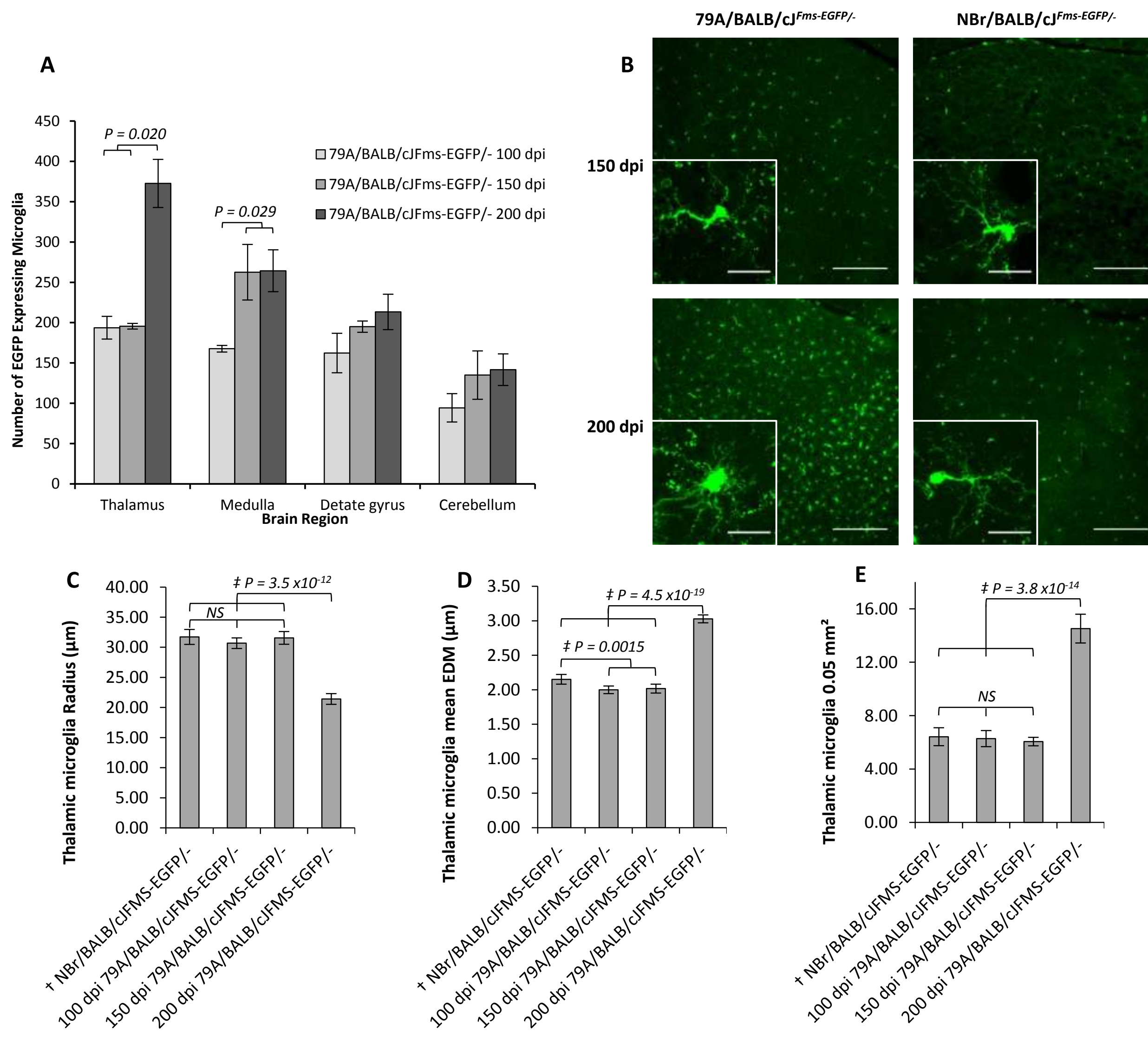

Accepted Manuscript Posted Online

Journal of Virology

JVI

Journal of Virology

Figure 5

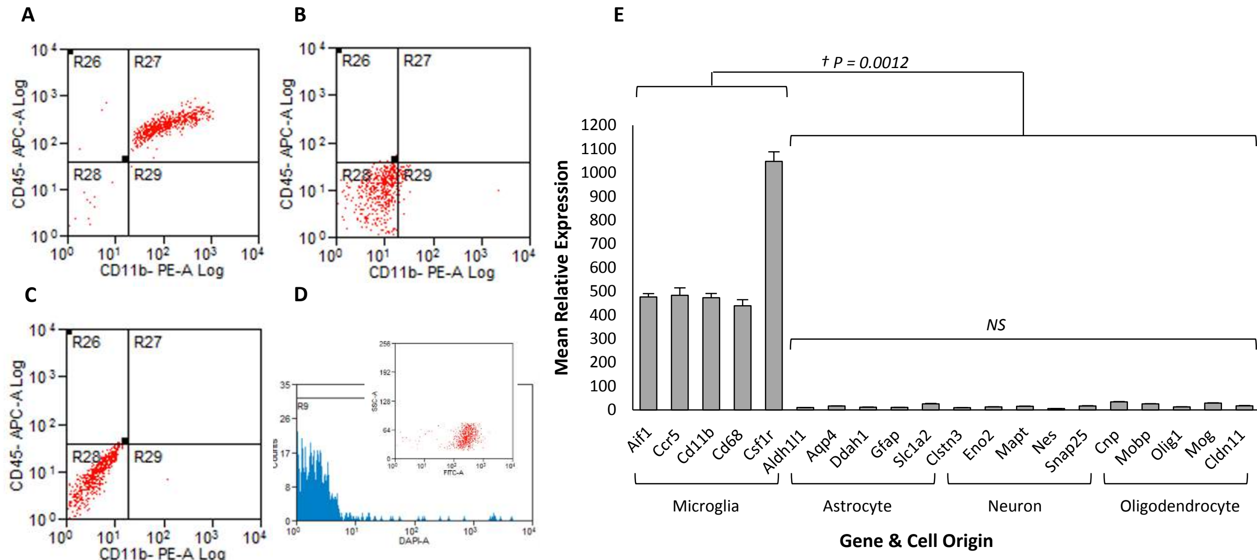

Accepted Manuscript Posted Online

Journal of Virology

JVI

Journal of Virology

Figure 6

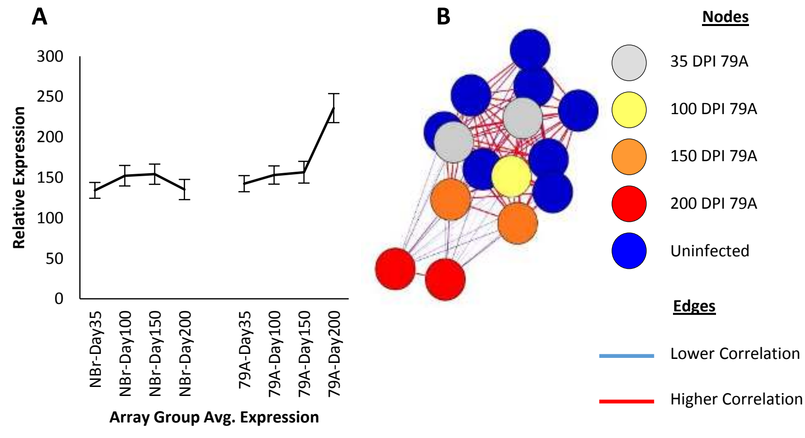

Accepted Manuscript Posted Online
JVI
Journal of Virology

Figure 7

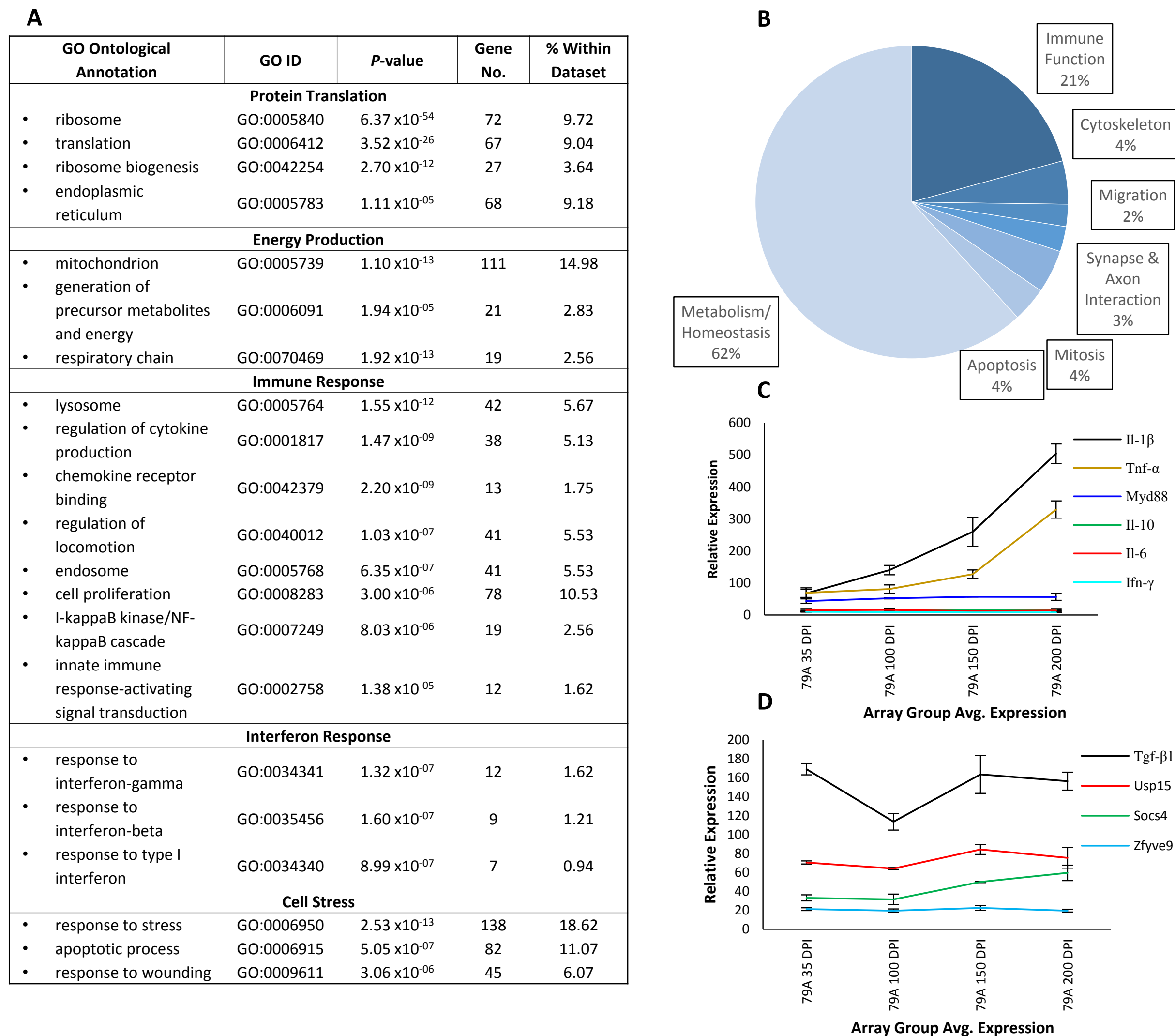

A

GO Ontological Annotation	GO ID	*P*-value	Gene No.	% Within Dataset
Protein Translation				
• ribosome	GO:0005840	6.37×10^{-54}	72	9.72
• translation	GO:0006412	3.52×10^{-26}	67	9.04
• ribosome biogenesis	GO:0042254	2.70×10^{-12}	27	3.64
• endoplasmic reticulum	GO:0005783	1.11×10^{-05}	68	9.18
Energy Production				
• mitochondrion	GO:0005739	1.10×10^{-13}	111	14.98
• generation of precursor metabolites and energy	GO:0006091	1.94×10^{-05}	21	2.83
• respiratory chain	GO:0070469	1.92×10^{-13}	19	2.56
Immune Response				
• lysosome	GO:0005764	1.55×10^{-12}	42	5.67
• regulation of cytokine production	GO:0001817	1.47×10^{-09}	38	5.13
• chemokine receptor binding	GO:0042379	2.20×10^{-09}	13	1.75
• regulation of locomotion	GO:0040012	1.03×10^{-07}	41	5.53
• endosome	GO:0005768	6.35×10^{-07}	41	5.53
• cell proliferation	GO:0008283	3.00×10^{-06}	78	10.53
• I-kappaB kinase/NF-kappaB cascade	GO:0007249	8.03×10^{-06}	19	2.56
• innate immune response-activating signal transduction	GO:0002758	1.38×10^{-05}	12	1.62
Interferon Response				
• response to interferon-gamma	GO:0034341	1.32×10^{-07}	12	1.62
• response to interferon-beta	GO:0035456	1.60×10^{-07}	9	1.21
• response to type I interferon	GO:0034340	8.99×10^{-07}	7	0.94
Cell Stress				
• response to stress	GO:0006950	2.53×10^{-13}	138	18.62
• apoptotic process	GO:0006915	5.05×10^{-07}	82	11.07
• response to wounding	GO:0009611	3.06×10^{-06}	45	6.07

Accepted Manuscript Posted Online
Journal of Virology
JVI
Journal of Virology

Figure 8

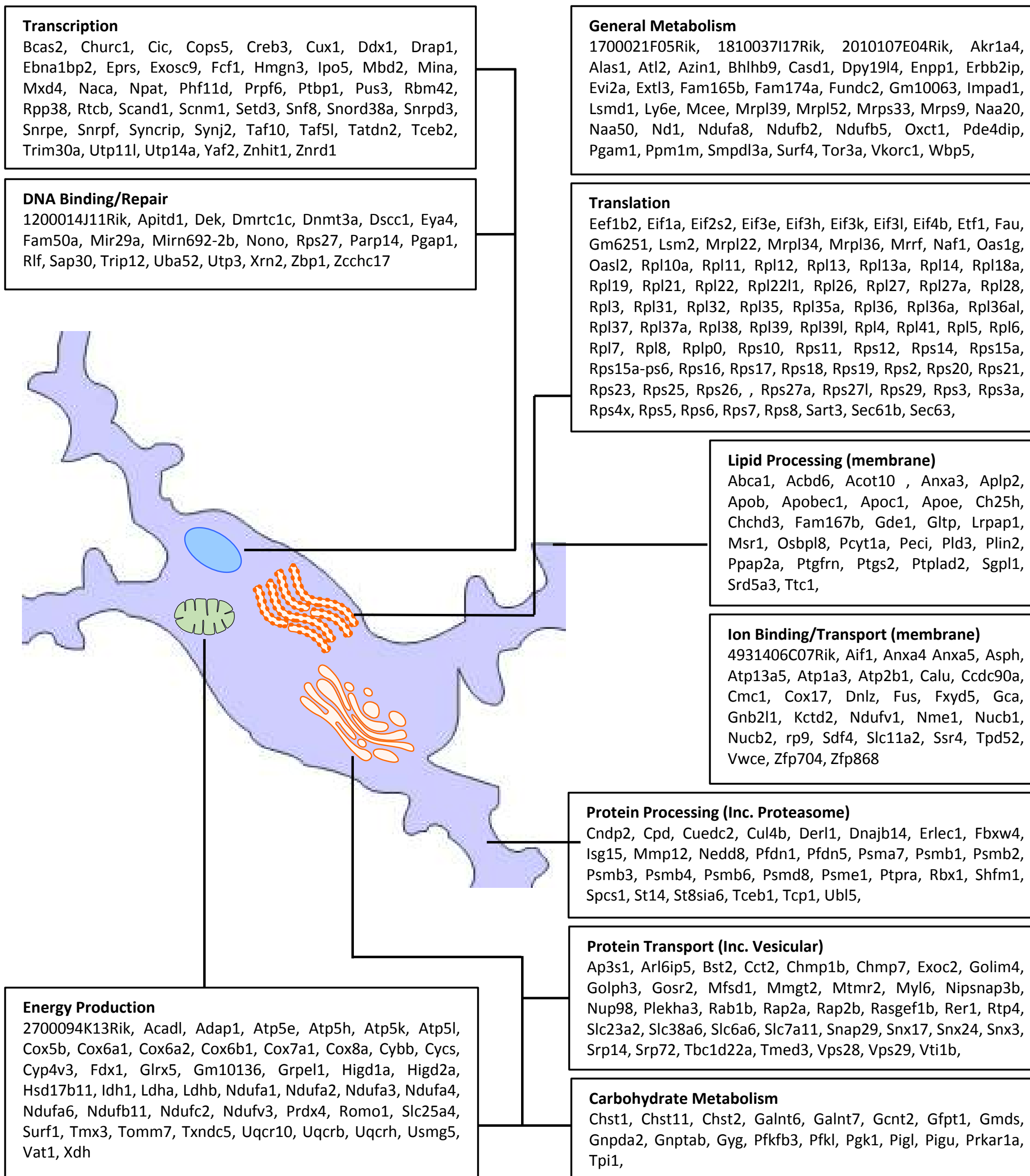

Accepted Manuscript Posted Online

Journal of Virology

JVI

Journal of Virology

Figure 9